Physical Properties of SmB_6 †

J. C. Nickerson* and R. M. White ‡
Department of Physics, Stanford University, Stanford, California 94305

and

K. N. Lee§ and R. Bachmann
Hansen Laboratories of Physics, Stanford University, Stanford, California 94305

and

T. H. Geballe|| and G. W. Hull, Jr.
Bell Telephone Laboratories, Murray Hill, New Jersey 07974

(Received 2 November 1970)

We propose a model for the electronic structure of SmB_6 suggested by new transport measurements in combination with analyses of the magnetic susceptibility and lattice energetics. Our model successfully describes the resistivity, Hall effect, magnetic susceptibility, and Mössbauer isomer shift in this material. In addition, it predicts an anomaly in the low-temperature specific heat. Analysis of the lattice energetics shows that the rigidity of the boron lattice is responsible for the fact that Sm ions on equivalent sites can occur with the $4f$ shell in either the $4f^5$ or the $4f^6$ configuration. A relationship among the compressibilities of the rare-earth hexaborides is predicted on the basis of this analysis.

I. INTRODUCTION

Samarium hexaboride is remarkable in that Sm ions on *equivalent* sites in SmB_6 can have their $4f$ shells in either the $4f^6$ or the $4f^5$ configuration, in the ratio $4f^6 : 4f^5 \cong 3 : 7$. This unusual situation has been established by measurements of the x-ray absorption,[1] resistivity and magnetic susceptibility,[2] lattice constant as a function of temperature,[3] and Mössbauer isomer shift.[4]

In order to interpret their resistivity and susceptibility data, Menth *et al.*[2] proposed that SmB_6 was a narrow-gap semiconductor in which Sm^{2+} ions ($4f^6$) were thermally ionized to produce Sm^{3+} ions ($4f^5$) and conduction electrons. Falicov and Kimball[5] lent theoretical support to such a model by showing that a qualitative fit to the resistivity was obtained when one included electron-hole interaction effects. This picture implied large changes in valence as a function of temperature. Three subsequent experimental results indicated, however, that this was not the case. First, our new transport data indicate that the change in carrier density accompanying the resistance change below 65 K is only a few percent of the number of Sm ions per cm^3. Second, because Sm^{2+} ions are larger than Sm^{3+} ions, one would expect an increasing lattice parameter with decreasing temperature. Although the lattice parameter does show a minimum at 150 K,[3] its increase below that temperature is much smaller than that expected from a substantial increase in the fraction of Sm ions in the $4f^6$ configuration. Third, the Mössbauer absorption line in ^{149}Sm nuclei in SmB_6 shows a peak part way between the positions characteristic of divalent and trivalent Sm ions, but the peak does not shift in the range 1–1000 K.[4] Cohen *et al.*[4] interpreted this result as demonstrating a temperature-independent mixture of $4f^6$ and $4f^5$ configurations, which, as they pointed out, is in apparent conflict with both the resistivity and susceptibility measurements.

We present a model for the electronic structure of SmB_6 based on mixed configurations, the transport data, and the susceptibility. This model, by emphasizing *configurational* rather than valence changes in the Sm ions, effectively decouples the transport and magnetic properties. In this way the apparent conflict between the Mössbauer and other measurements is resolved. In addition, the model predicts an anomaly in the low-temperature specific heat.

In Sec. II, we present our transport measurements and describe the aspects of the model which they suggest. In Sec. III, we present our analysis of the magnetic properties and from this analysis identify the bands introduced in Sec. II. We analyze the lattice energetics in Sec. IV, showing that the rigidity of the boron lattice provides a physical explanation of the mixed configurations. Finally, in Sec. V, we discuss the specific heat and present our measurements.

II. ELECTRONIC STRUCTURE

A. Experimental

Metal borides exist over a wide range of atomic

ratios, so that it is difficult to obtain single-phase material. In addition, the rigidity of the boron lattice permits large deviations from stoichiometry, especially metal deficiency.[6] We have prepared SmB_6 samples by two methods: (i) The elements, in stoichiometric proportions, were sintered at about 1600°C in tantalum or tungsten crucibles sealed off under vacuum; the resulting granular material was then remelted in an arc furnace to obtain homogeneous samples of the correct density. (ii) Layers of SmB_6 were grown on boron crystals by evaporating Sm metal on boron substrates, which were then heated to about 1800 °C. Metallographic and x-ray analysis showed all the material to be single phase. As we discuss below, the quality of the material is most easily assessed by its low-temperature conductivity. We attribute the residual conductivity to Sm deficiency on the basis of our transport data.

We have measured the resistivity and Hall effect in the range 1–300 K using alternating sample current and a Princeton Applied Research HR-8 lock-in amplifier. The samples were rectangular in shape, typically 6 mm long and 2 mm wide. Leads were attached in the ordinary 5-lead configuration. While the resistivity could be measured readily, the detection of the small Hall voltage involved some difficulties.

The brittleness of SmB_6 prevented us from lapping bulk samples thinner than about 1 mm, thus limiting attainable current densities. This difficulty prompted us to grow SmB_6 in the form of thin layers on boron crystals. The thinness of these layers (about 3 μm as estimated from the room-temperature resistivity of bulk SmB_6) made it easier to measure the Hall effect over the whole temperature range.

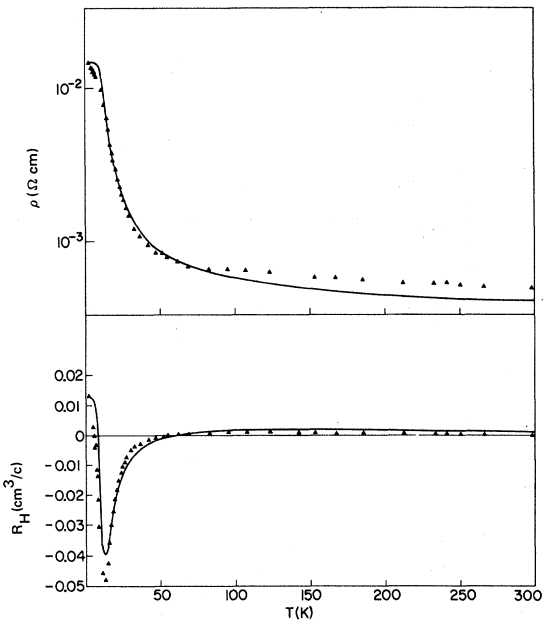

FIG. 1. Resistivity and Hall coefficient of SmB_6 layer sample in the range 0–300 K. The solid curves are from a calculation described in the text.

Figure 1 shows the resistivity and Hall coefficient as a function of temperature in a SmB_6 layer. The room-temperature value of the resistivity has been normalized to 5×10^{-4} Ω cm. Such a normalization is justified by our experience that the high-temperature resistivity of SmB_6 is, within a factor of 2, unaffected by sample preparation, or even by intentional doping with europium or gadolinium.[7]

Figure 2 shows the resistivity and Hall mobility of both layer and bulk samples in the range 1–75 K. As in the earlier study,[2] the resistivity drops sharply between 10 and 50 K. While the qualitative features of resistivity and Hall mobility are similar in the two samples, the layer resistivity below 4 K is lower than that of the bulk by more than one order of magnitude. Paderno *et al.*[8] measured the thermoelectric voltage as a function of temperature in SmB_6 and observed low- and higher-temperature crossings similar to the Hall mobility.

B. Band Model

On the basis of tight-binding calculations, Longuet-Higgins and Roberts[9] showed that the boron lattice of a hexaboride requires two electrons per formula unit (in addition to the boron electrons) to achieve chemical stability. The metal ions in the rare-earth hexaborides are generally trivalent, and thus these compounds are metallic. SmB_6 and EuB_6, however, contain divalent ions, and these are semiconductors.[10]

From the transport data shown in Fig. 2 one can straightforwardly infer a band scheme to describe the semiconducting properties of SmB_6. In interpreting the Hall measurements we have made no corrections for magnetic or many-body effects,[11] primarily because there is no magnetic ordering in SmB_6.[2,12]

Below 3 K, the resistivity is constant and of the order of 10^{-1} Ω cm. At these low temperatures the Hall mobility is small and positive, about +1 cm^2/V sec. The data we show are typical of all the samples we have measured in the sense that, while the value of the resistivity is sample dependent, the value of the Hall mobility below 3 K is not. Therefore, we attribute the residual conductivity to hole conduction arising from Sm deficiency, and infer the presence of an almost-filled valence band derived from Sm-ion states.

Near 6 K, the Hall mobility switches sign, and at roughly the same temperature the resistance drop accelerates. This implies the presence of a conduction band separated from the valence band by a

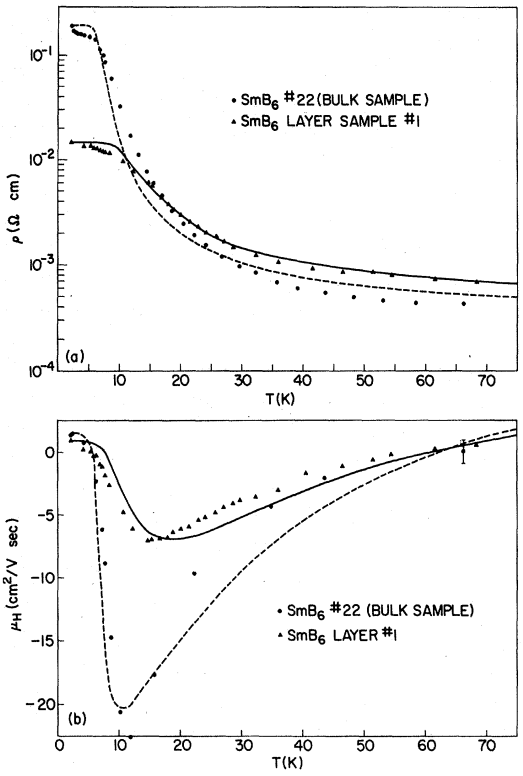

FIG. 2. Resistivity and Hall mobility of SmB_6 samples in the range 0–75 K. ●, bulk sample; ▲, layer sample. Calculated curves are discussed in text.

small (~ 25 K) band gap. The peak in the (negative) Hall mobility at about 15 K shows the mobility in the conduction band to be $\gtrsim 20$ cm²/V sec.

Two bands, however, are not enough to describe the transport data, as evidenced by the peak in the Hall mobility. Above 15 K, the Hall effect indicates the introduction of high-mobility hole carriers, such that by about 65 K the Hall coefficient crosses zero again. These carriers, having mobilities of order 100 cm²/V sec, are attributed to a second valence band lying lower than – though close to – the upper valence band. The mobilities necessary for a second zero crossing are high because the resistivity in the region near and above 65 K is relatively flat. This behavior indicates that the Fermi level is well up in the conduction band, and thus the hole population in the lower band arises only from the Boltzmann tail of the Fermi distribution.

In fact, in the range above 50 K, the slow variations in the resistivity and Hall coefficient are characteristic of semimetals. We may describe SmB_6 as a system which changes from a semiconductor to a semimetal in the region 40–60 K.

These qualitative considerations suggest the energy-band diagram of Fig. 3. Before fitting the parameters of this model to the resistivity and Hall effect, it is worth pointing out that the total change in carrier concentration accompanying the resistivity change below 65 K is relatively small. As a rough estimate, we take the conduction-band mobility to be 20 cm²/V sec at 20 K, and use this figure as a mean value for the mobility.[13] In such a case, the bulk resistivity of about 10^{-3} Ωcm at 65 K implies a carrier concentration of order 10^{20} cm^{-3}; most of these will be conduction-band electrons, but their number still amounts to only a few percent of the number of Sm ions per cm³.

Such a small change in carrier concentration appears to resolve the conflict between the Mössbauer and other measurements, but in fact the size of the carrier change is not relevant to the Mössbauer experiment. The transport measurements are primarily sensitive to changes of *valence*, i.e., carrier concentrations. On the other hand, the susceptibility and Mössbauer isomer shift are sensitive to changes in *configuration*, which do not necessarily alter valence. Earlier work[2] assumed that changes in valence and configuration were equivalent, and it is this assumption which we discard in our model.

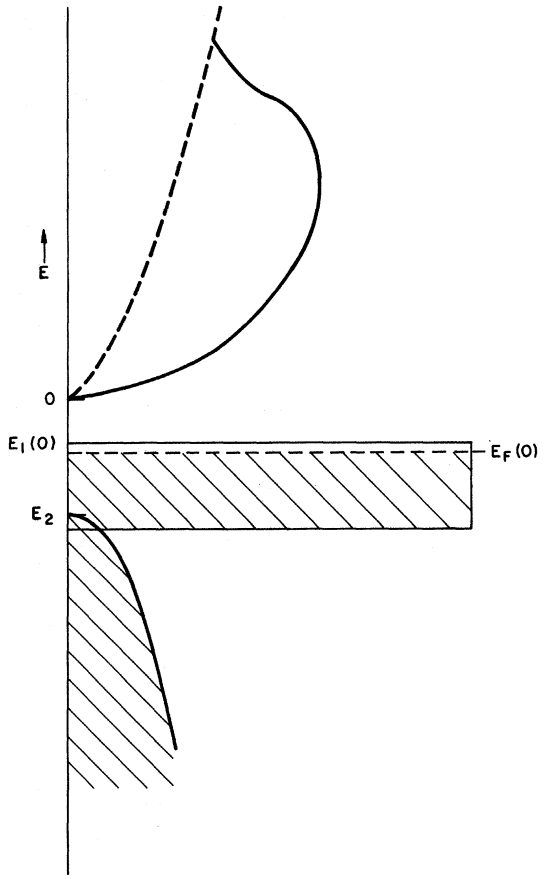

FIG. 3. Schematic energy-band diagram for SmB_6.

C. Calculation of Resistivity and Hall Effect

The conductivity in our three-band model is given by

$$\sigma = (n\mu_n + p_1\mu_1 + p_2\mu_2)\,|e|\,, \tag{1}$$

where n is the number of electrons per cm^3 in the conduction band, with mobility μ_n, and p_i is the number of holes per cm^3 in the ith valence band, with mobility μ_i. The Hall coefficient is given by

$$R_H = \frac{-n\mu_n^2 + p_1\mu_1^2 + p_2\mu_2^2}{(n\mu_n + p_1\mu_1 + p_2\mu_2)^2\,|e|}\,, \tag{2}$$

and the Hall mobility is related to these quantities by

$$\mu_H = R_H\sigma = \frac{-n\mu_n^2 + p_1\mu_1^2 + p_2\mu_2^2}{n\mu_n + p_1\mu_1 + p_2\mu_2}\,. \tag{3}$$

We shall now show that by using reasonable parameters Eqs. (1)–(3) give a good fit to the observed data. These parameters are not unique; nonetheless, they are restricted quite severely by the measurements. Thus, the energy gaps must obey 20 K $< |E_1| < |E_2| <$ 100 K in order to reproduce the low-temperature resistivity change.

We have assumed that the lower valence band and the conduction band have parabolic shape, i.e., their densities of states have the form

$$N(\epsilon) = \frac{d}{4\pi^2}\left(\frac{2m^*}{\hbar^2}\right)^{3/2}|\epsilon - \epsilon_0|^{1/2}\,, \tag{4}$$

where ϵ_0 is the band edge, d is the band degeneracy, and m^* is the effective mass. The upper valence band is treated as a broadened level with a constant density of states, $N(\epsilon) \propto 1/B$ (B equals bandwidth). The carrier concentrations in the bands are then given by

$$\left(\frac{n}{p}\right) = \int_{\text{band}} \frac{N(\epsilon)\,d\epsilon}{1 + e^{\pm(\epsilon - \epsilon_F)/kT}}\,. \tag{5}$$

The effective masses (i.e., bandwidths) of the two high-mobility bands are fixed by the value of the resistivity and Hall coefficient at high temperatures, as well as by the $T \approx 65$ K crossing temperature of the Hall mobility. The width of the narrow band is small, and it is unimportant, since we use the narrow band mainly in the determination of ϵ_F.

The mobilities of the conduction and lower valence bands are also qualitatively determined by the transport data, as indicated above; that of the narrow valence band is fixed by the Hall mobility at the lowest temperatures. In preliminary computations we found that the transport behavior could be qualitatively reproduced with constant mobilities, the two crossings and the peak of the Hall mobility appearing at the proper places, and the resistance drop occurring in the right temperature range. In order to make a quantitative fit we improved the earlier calculation by giving the mobilities temperature dependence in the phenomenological formula

$$\mu(T) = \frac{\mu_0}{1 + (T/T_0)^\alpha}\,, \tag{6}$$

where T_0 is a characteristic temperature about $\frac{1}{30}$th of the Debye temperature. The exponent α is taken to be $\frac{3}{2}$ for the valence bands and 1 for the conduction band. Because of the high Debye temperatures of the hexaborides, Eq. (6) has little effect on the low-temperature behavior, but it does cause μ_H to fall faster toward zero above 30 K, and remain small thereafter. We attach no physical meaning to the exponents α, nor to the form we have chosen for the mobility; apart from phonon scattering, a study of the spin susceptibility of the $4f^6$ Sm ions[14] indicates that spin-disorder scattering may play an important role in determining the behavior of the mobility. Further microscopic calculations are in progress.

There is a remaining subtlety, introduced by the fact that the upper narrow valence band is a tight-binding-like band derived from the divalent Sm ions (see Sec. III). The electrons here are highly correlated, giving rise to states characterized by their total angular momentum J. As we show in an Appendix, this correlation may be accounted for by treating the narrow band as a broadened level, whose energy relative to the bottom of the conduction band is temperature dependent. This dependence is given by

$$E_1(T) = E_1(0) + kT(\ln Z_3 - \ln Z_2)\,, \tag{7}$$

where Z_3 and Z_2 are the partition functions for the trivalent and divalent Sm ions, respectively. The energies entering the sums over states are measured relative to the appropriate ground-state configuration energies.

We have computed the resistivity and Hall effect for various combinations of the parameters. Two separate fits were carried out, using the data from a bulk sample and from a layer sample. With parameters chosen as in Table I, we find the calculated curves of Figs. 1 and 2.

The difference in mobilities between the two samples is consistent with a higher impurity (defect) concentration in the layer sample. The large effective mass of the conduction-band electrons is noteworthy, and it will be discussed in Sec. III.

In view of the strong variations of the Hall effect and the resistivity, we believe that the good agreement between this calculation and the experimental data lends strong support to the proposed model for the electronic structure of SmB_6.

III. SUSCEPTIBILITY

The measurements of Paderno *et al.*[15] and of

TABLE I. Band and transport parameters for the three-band model. Numbers in parentheses are those used to fit the data from the layer sample, while the others are for the bulk sample.

	Conduction	Upper valence band	Lower valence band
Mobility at $T=0$ (cm^2/Vsec)	35 (21 5)	1.45 (0.9)	390 (265)
Effective mass (m^*/m_e)	25.2 (25.2)	...	3.1 (3.1)
Bandwidth (K)	1100 (1100)	100 (100)	9000 (9000)

Fraction of holes at $T=0$: 0.17% (3.3%) number of Sm ions

Energy gaps: $E_1(0) = -49$ K (-30) $E_2 = -81$ K (-81)

Menth *et al.*[2] showed that the high-temperature susceptibility of SmB_6 falls between the susceptibilities of the $4f^6$ and $4f^5$ configurations. Initially, then, one would suppose that a mixture of these two would explain the measurements. Since the $4f^5$ is magnetic, its susceptibility should show a Curie-Weiss–type divergence, and, at sufficently low temperatures, a system of $4f^5$ ions should order. Menth *et al.*, finding no ordering down to 0.35 K and no divergence down to 1 K, concluded that $4f^5$ ions were not present at low temperatures.[2]

The lattice-constant measurements of Levinstein[3] showed, however, an order of magnitude less increase at low temperatures than would be expected if the fraction of trivalent $4f^5$ ions at room temperature were to lose its magnetism by becoming divalent $4f^6$. This result, combined with the discovery of a fixed $4f^6:4f^5$ ratio by Cohen *et al.*[4] made the magnetic behavior anomalous.

The fact that the Sm-Sm distance in SmB_6 is abnormally large compared to the trivalent rare-earth hexaborides[16] makes it reasonable to consider the possibility of a second divalent configuration, one made up from the $4f^5$ core plus a hybridized $5d$-$6s$ electron state.[17] Such a configuration would be easy to ionize, accounting for the small value of the energy gap E_1. Further, the $4f^5$-like ionic radius of this configuration would not cause appreciable lattice-constant change upon ionization. Also, as pointed out by Cohen *et al.*,[4] the Mössbauer isomer shift is more directly influenced by the number of $4f$ electrons than by the number of $5d$ or $6s$ electrons, so that the absence of a shift in the Mössbauer peak is explained in this scheme. Finally, as we show below, the ground-state level of the $4f^5(5d\text{-}6s)$, treated as a configurational entity, has $g_J=0$. That is, although $J\neq 0$, the spin and orbital magnetic moments cancel identically. Thus, with this configuration we are able to explain the magnetic behavior quantitatively, while retaining an interpretation consistent with all the observed data in other measurements.

A. Analysis

1. $4f^5(5d\text{-}6s)$ *Configuration*

The $5d$-$6s$ electron state derives from the corresponding levels of the free Sm^{2+} ion. Its magnetic character is strongly influenced by the cubic crystal field of SmB_6. The crystal field splits the $5d$ orbitals into a low-lying *nonmagnetic* e_g doublet and a higher magnetic t_{2g} triplet, with a splitting of the order of electron volts.[18] The t_{2g} states are thus unimportant below 10^4 K. The e_g states have no orbital angular momentum, so that our model $5de_g$-$6s$ electron looks like an s electron magnetically, with only a spin moment. For brevity, then, we shall call the $4f^5(5de_g\text{-}6s)$ ionic configuration f^5s.

We shall discuss the energetics of the f^5s at length below, but first we compute the ground-state moment. The $5d$-$6s$ spin can couple either parallel or antiparallel to the $4f^5$ core spin. According to Hund's rules, the core spin is $\frac{5}{2}$, and for ferromagnetic exchange between core and $5d$-$6s$, the parallel arrangement with $S=3$ will be the term containing the ground level. The ground level, by another application of Hund's rules, will be the one with $J=L-S=2$. Applying the standard Landé formula, we find $g_{J=2}=0$, as stated above. This is an interesting result, that although the angular momentum is nonzero, its associated magnetic moment vanishes. We assume that Sm ions in stoichiometric SmB_6 are in either the $4f^6$ or f^5s configuration at $T=0$, so that there is no divergence of χ at low temperatures.

We describe the f^5s configuration by the Hamiltonian

$$\mathcal{H}=\mathcal{H}_0+A_5\vec{L}_5\cdot\vec{S}_5-\mathcal{J}_{ex}\vec{S}_5\cdot\vec{s}\ . \tag{8}$$

$\mathcal{H}_0$ is the spin-independent part. $\vec{L}_5$ and $\vec{S}_5$ are the total orbital and total spin angular momentum operators for the f^5 core, and $\vec{s}$ is the spin operator for the $5de_g$-$6s$ electron.

In contrast to the ordinary case, where $\mathcal{J}_{ex}$ is so large that one is confined to a single L-S term, we must explicitly include the exchange term here because it may be comparable to the spin-orbit energy of the $4f^5$ core. In the usual case of a configuration comprising equivalent electrons, Hund's rules require one to maximize the total spin before maximizing L and coupling these to obtain J values. In the f^5s configuration, however, $\mathcal{J}_{ex}$ will be considerably smaller because the localized state and the core states belong to different shells, so that the overlap is decreased.

We choose the $|LSL_zS_z\rangle$ representation as a basis for diagonalizing the Hamiltonian (8). This amounts to diagonalizing the exchange term first, so that we have L-S terms for the whole f^5s configuration. The ground term of the $4f^5$ core is $L_5=5$, $S_5=\frac{5}{2}$. Coupling this to the $l=0$, $s=\frac{1}{2}$, $5de_g$-$6s$ electron, we find two terms: the $L=5$, $S=3$, $f^5s\|$, in which the core and localized spins are parallel; and the antiparallel $L=5$, $S=2$, $f^5s\#$.

In order to find the actual energy level structure we must then diagonalize the spin-orbit interaction. The symmetry of $\mathcal{H}$ permits us to label the levels by the total angular momentum quantum number J. Note, however, that the spin-orbit term mixes levels of the same J, but different S. The small size of J_{ex} suggests that these pairs of levels may be close enough to be mixed significantly. We emphasize that this mixing does not affect the lowest- and highest-lying ($J=2$ and 8) levels of the $f^5s\|$ because $3\leq\mathcal{J}\leq 7$ in the $f^5s\#$ term. In particular, the $J=2$ ground level, which has vanishing moment, is unaffected.

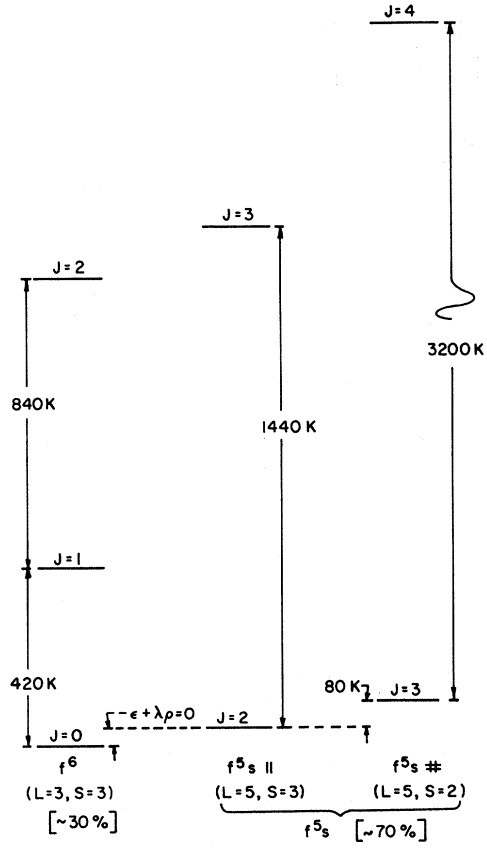

FIG. 4. Energy-level diagrams for divalent Sm-ion configurations. Level spacings are determined from the observed susceptibility, except for the splitting between f^5s and $4f^6$ ground levels, which is determined by the lattice considerations of Sec. IV.

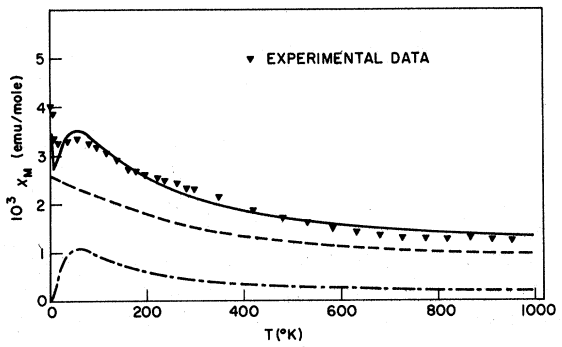

FIG. 5. Susceptibility of SmB_6 in the range 0–1000 K. Experimental data points are taken from Ref. 2. Solid curve is the theoretical fit described in the text. Dashed curve shows the sum of the susceptibilities of the $4f^6$ and $f^5s\|$ configurations, which account for the bulk of the susceptibility. The dot-dashed curve is the contribution due to the $f^5s\#$ term. Note that the bare $4f^5$ contribution is responsible for the weak divergence below 20 K.

In order to take this mixing into account in our model, we allow the spin-orbit parameters to be adjustable, starting from estimates made for the free Sm^{3+} ion.[19]

On the right-hand side of Fig. 4 we show the four lowest-lying levels of the f^5s configuration, which, following the x-ray absorption and Mössbauer data,[1,2] we take to comprise 70% of the Sm ions. The level spacings shown are determined from our fit to the observed susceptibility,[2] as discussed below. The small distance between the two lowest-lying f^5s levels gives rise to a contribution to χ from the $f^5s\#$ $J=3$ state, which is magnetic. In our calculations this is responsible for the hump in the susceptibility near 100 K (Fig. 5). On the left-hand side of Fig. 4 we show the level scheme for the divalent $4f^6$ configuration, with spacings determined again from the fit to the experimental data.

2. *Calculation of* χ

The susceptibility is the sum of the various Sm-ion-term susceptibilities, weighted by the probabilities that the terms are occupied:

$$\chi(T)=\textstyle\sum_i \rho_i \chi_i\,, \tag{9}$$

where i denotes $4f^6$, $f^5s\|$, $f^5s\#$, or $4f^5$ L-S terms, and the χ_i are calculated from the well-known formula of Van Vleck[19]

$$\chi_i(T)=\sum_{J=|L-S|}^{L+S}\left(\frac{g_J^2\beta^2J(J+1)}{3kT}+\alpha_J\right)(2J+1)e^{-W_J/kT}\Big/ \sum_J(2J+1)e^{-W_J/kT}\,. \tag{10}$$

The ρ_i are determined as follows: For the two f^5s

terms we use Boltzmann factors to determine their relative populations; the $4f^6$ fraction is fixed at about 30% by the lattice considerations of Sec. IV; and the $4f^5$ fraction is taken to be the number of carriers plus a fixed fraction (2%) of the Sm ions per cm^3. We associate the fixed fraction with the number of holes at $T=0$ in the narrow valence band (see below).

We see that the susceptibility depends explicitly on the energy levels W_J. The temperature-independent contributions α_J are also determined by these energy levels if we ignore effects arising from the mixing of the $f^5s\,\|$ and $f^5s\,\#$ levels. As this mixing does not significantly influence the quantitative calculation, these approximate α_J suffice. In similar fashion, the g_J are computed from the Landé formula, again ignoring spin-orbit–induced mixing of the $J=3$ to 7 levels. The relative populations of the $f^5s\,\|$ and $f^5s\,\#$ are calculated from the W_J as well. The W_J are taken to be of the form[19] $A_i J(J+1)$ apart from a constant depending on L and S; the A_i are the spin-orbit parameters for the various terms.

We have further modified Eq. (10) to include the effects of the crystal field on the ground levels of the $4f^5$ and f^5s terms. The crystal field splittings were estimated using a point-charge plus conduction-electron model for the bare $4f^5$ ion, and a self-induced crystal field due to the $5d$-$6s$ electron for the f^5s.[18] The crystal field effects are important only for obtaining a precise fit to the hump in χ due to the excitation of the $f^5s\,\#$.[20] The qualitative behavior of the susceptibility is dominated by the $J=0$ and $J=1$ levels of the $4f^6$, neither of which is split by a cubic field.

The A_i are therefore the main adjustable parameters. *Ab initio* estimates of the spin-orbit parameters for the $4f^6$ and bare $4f^5$ configurations have been made by Van Vleck[19]; both are about 400 K. From the $4f^5$ value, we may extract the A_i for the f^5s by recalling that the spin-orbit energy in both configurations is the same. Again the estimates lie near 400 K. We have permitted all the A_i to vary. The calculated curve of Fig. 5 is obtained using the spin-orbit parameters of Table II. The values are in good agreement with the initial free-ion estimates except for the $f^5s\,\#$ term, where the interterm mixing seems to be important.

The agreement between the experimental data[2] and our calculated curve is good except perhaps at very low temperatures, where the possible presence of magnetic impurities makes the interpretation of the measurements less certain. As one can see from the partial susceptibilities plotted in Fig. 5, the $4f^6$ and $f^5s\,\|$ dominate the susceptibility throughout the temperature range; the $4f^6$ makes up the major part of this contribution. These terms display Van Vleck temperature-independent susceptibility below 100 K, a fact which is partially masked by the increase in $f^5s\,\|$ population with decreasing temperature. The hump in the calculated susceptibility near 100 K is due to the excitation of the $f^5s\,\#$ $J=3$ level, as noted before.[21] The bare $4f^5$, with its Curie-like susceptibility, is negligible except at the lowest temperatures, where a weak divergence is suggested by the measurements.

We have thus achieved a quantitative fit to the magnetic susceptibility, using an ionic model based upon the unusual f^5s configuration. The connection between these ionic localized states and the bands in our model of the transport properties then completes our description of SmB_6.

B. Identification of Bands

Our band scheme in Sec. II was derived from the transport data, except for the unimportant temperature dependence of the upper valence band. The susceptibility fit is independent of the band scheme as well, taking from the transport only the number of $4f^5$ ions at $T=0$, corresponding to the number of Sm-deficient metal sites. We are now in a position to identify the bands with ionic configurations.

From its large mobility we infer that the lower valence band is derived from boron bonding ligands.[16,22] Johnson and Daane studied the alkaline-earth hexaborides,[23] and showed that the conduction band (which is probably the antibonding band in these materials) lies about 0.4 eV above the top of the bonding band. Our small bandgaps suggest, then, that the upper valence and conduction bands in SmB_6 originate from the Sm ions.

We identify the conduction band with a set of *delocalized* $5d$-$6s$ electron states. Near the band edge this band is presumed to have pronounced d character, which accounts for the unusually high effective mass and narrow bandwidth assigned to the conduction band in the fit of the transport measurements. Such an identification is supported by the resistivities of other rare-earth hexaborides,[22] which have values similar to those found in d-band metals. In addition, the crystal field splittings in the other rare-earth hexaborides are correctly predicted by assuming that the conduction bands in these materials have $5de_g$-like character.[18]

The narrow valence band is identified with the

TABLE II. Spin-orbit parameters for the configurations of the Sm ion in SmB_6.

Ground-state term	$4f^6$ ($L=3$, $S=3$)	$f^5s\,\|$ ($L=5$, $S=3$)	$f^5s\,\#$ ($L=5$, $S=2$)	$4f^5$ ($L=5$, $S=5/2$)
Spin-orbit parameter (K)	420	480	800	500

localized states. The precise nature of this correspondence is rather subtle because the strong electron correlations in the ionic configurations require modification of the one-electron picture which underlies the band concept. The band properties of such a collection of states are inferred from the form of the partition function for the whole system, as detailed in the Appendix; as mentioned before, the net effect is to give a temperature dependence to the position of the band.

Another remark may be made concerning the narrow band. The motion of the band derives from the redistribution of population among the various ionic energy levels as kT rises. In principle, the $4f^6$ could ionize thermally in the same manner as the f^5s configuration. As we discuss further below, however, the strain and configuration energies enforce a fixed $4f^6 : 4f^5$ f-shell ratio for temperatures up to 1000 K,[4] so that this ionization process is strongly inhibited.

In our case, the motion of the narrow band has no qualitative effect on the transport behavior. Inclusion of the motion, which lowers the band gap with increasing temperature, necessitates choosing a larger $T=0$ value for $|E_1|$ in order to fit the resistivity data.

In summary, our analysis shows that the magnetic susceptibility is independent of valence changes ($4f^6$ or $f^5s \rightarrow 4f^5$ transitions), originating instead from the fixed $4f^6$ fraction and from $f^5s\,\| \rightarrow f^5s\,\#$ *configurational* transitions. By contrast, the transport properties *are* strongly dependent on valence changes, since the conduction electrons result almost entirely from $f^5s \rightarrow 4f^5$ transitions.

IV. FIXED $4f^6 : 4f^5$ RATIO

The x-ray absorption,[1] lattice constant,[3] and Mössbauer[4] studies of SmB_6 show that it contains ions with $4f^6$ and $4f^5$ f-shells in a ratio of about 3 : 7 over a wide range of temperatures. The Sm sites, however, are presumably equivalent. We now show how the rigidity of the boron lattice provides an explanation for this remarkable fact.

Briefly, our argument is as follows: Because of the rigidity of the boron network, a small change in the size of the unit cell gives rise to a large change in lattice strain energy. The two Sm-ion configurations[24] are of different sizes, the $4f^5$ being smaller. The SmB_6 crystal can then minimize its total free energy by a compromise in which the ions have a mixture of two configurations.

The metal ions in the hexaborides sit at the body centers of the unit cells. At each corner there is a relatively large boron octahedron. The physical properties of the hexaborides resemble those of elemental boron, as one might expect with such an open boron network: The hexaborides are very hard, have high melting points ($\approx 2200\,^\circ$C), small coefficients of expansion, and, significantly, lattice constants which lie within 2% of 4.15 Å.[16,22] These facts, especially the last, indicate the rigidity of the boron network and its resistance to changes in unit-cell dimension.

The other contributing factor is the configuration energy. Compared with the lighter rare earths, Sm has a smaller divalent-to-trivalent ionization energy because of the tendency to fill the $4f$ orbital subshell as much as possible. In the more extreme case of europium, one finds a pronounced tendency for Eu ions to be divalent, as they are in EuB_6.[16]

A. Lattice Energetics

We quantify our argument with a simple spring model which takes into account the boron-boron and boron–rare-earth interactions which give rise to the strain energy. Our reason for using such a picture rests on the belief that, to lowest order, the role of the rare-earth ion is geometrical. The parameters defining our model may then be evaluated for SmB_6 and applied to predict the compressibilities of the other rare-earth hexaborides.

The total energy has two contributions, E_c, the configuration energy, and E_h, the hexaboride strain energy. E_h is a function of both the lattice constant a and the metal-ion radius r. For an ion of given radius, the strain energy will vary with variations of the lattice constant (a sort of compressibility-experiment picture). Conversely, for fixed a, E_h will vary with ionic radius because of the boron–rare-earth interaction. We emphasize that our model is crude here, as we reduce wave-function-overlap effects to two parameters.

We make the reasonable assumption that there are values of a and r which minimize the strain energy. Thus, expanding E_h about these ideal values a_0 and r_0 and retaining only the quadratic terms, we find that

$$E_h = \tfrac{1}{2}C_a(\Delta a)^2 + \tfrac{1}{2}C_r(\Delta r - \alpha\Delta a)^2 \,. \tag{11}$$

C_a, C_r, and α are the second derivatives of E_h evaluated at (a_0, r_0) in the usual way; $\Delta a = a - a_0$, $\Delta r = r - r_0$.[25] We have chosen the zero of energy at $E_h(a_0, r_0)$.

E_h depends on the mixture of $4f^6$ and $4f^5$ ions through the ionic radius r. We denote the fraction of $4f^6$ ions ρ; the average ion radius is then

$$r = \rho(r_5 + \delta r) + (1-\rho)r_5 = r_5 + \rho\delta r \,, \tag{12}$$

where r_5 is the $4f^5$ ion radius and $\delta r = r_6 - r_5 > 0$ is the difference between $4f^6$ and $4f^5$ ion radii.

The configuration energy in the mixed-f-shell case is a similar average:

$$E_c = E_5 + \rho\delta E \,, \tag{13}$$

where E_5 is the $4f^5$ energy and $\delta E = E(4f^6) - E(4f^5)$. Putting (12) into (11) and minimizing with respect to

a, we have a total energy which takes the form

$$E = E_h + E_c = E_0 - \epsilon\rho + \tfrac{1}{2}\lambda\rho^2 . \tag{14}$$

Minimizing with respect to ρ, we find that

$$\rho = \epsilon/\lambda , \tag{15}$$

so that if $0 < \epsilon < \lambda$, there will be a mixture of $4f^6$ and $4f^5 f$-shells at $T = 0$. Putting in the explicit forms for ϵ and λ, the condition for a mixed configuration becomes

$$r_5 < r_0 - [\delta E/C_r(\delta r)^2]\xi\delta r < r_6; \quad \xi = 1 + \alpha^2 C_r/C_a . \tag{16}$$

For $T \neq 0$ we must minimize the free energy. If the entropy is given simply by the configurational entropy arising from the two different species of ions, then ρ will change significantly when $\lambda/kT \approx 1$. Applying these results to SmB_6, we would set $\rho(T=0) \approx 0.3$, $\lambda \gtrsim 1000$ K, in order to reproduce the lattice-constant[3] and Mössbauer[4] measurements.

Note that the rigidity of the boron lattice enters our argument at two places. First, in order for the expansion (11) to be valid, Δa and Δr must be small; the small variation of the lattice constant among all the hexaborides suggests that this condition is plausible.[26] Second, of course, (16) must be satisfied, which requires $C_r(\delta r)^2 \approx \delta E$ in order that the last term contribute to ρ without dominating it.

In order to gain more perspective on the mixed-f-shell phenomenon, we may calculate the energy separation between the $4f^6$ and $4f^5$ (really, the $f^5 s$) configurations, taking the lattice energy into account. To do this, we note that the total energy in Eq. (14) is a function of a and ρ; keeping a fixed at its equilibrium value and allowing ρ to vary, we may then minimize the free energy at finite temperature. We find for the effective energy separation that

$$[E(4f^6) - E(4f^5)]_{\text{eff}} = -\epsilon + \lambda\rho. \tag{17}$$

This is the energy separation drawn in Fig. 4. At equilibrium we have $\rho = \epsilon/\lambda$ at $T = 0$, as in (15).

B. Compressibilities

We may now compute the compressibility κ using

$$\frac{1}{\kappa} = -V\left(\frac{\partial p}{\partial V}\right)_T = V\left[\frac{\partial}{\partial V}\left(\frac{\partial E}{\partial V}\right)_S\right]_T, \tag{18}$$

where the first derivative is taken at constant ρ (constant S), and in taking the second at constant T we allow ρ to vary, adjusting to its isothermal value. From (11) and (13) we find that if $0 < \rho < 1$,

$$\kappa = 9\,a/C_a, \tag{19a}$$

while if ρ is fixed at 0 or 1,

$$\kappa = 9a/C_a\xi . \tag{19b}$$

Physically, we expect C_a to be independent of metal ion for all the hexaborides. On the other hand, ξ will depend on which rare-earth hexaboride we consider. We make the assumption that ξ depends mainly upon the presence or absence of conduction electrons, so that ξ has a characteristic value for metallic hexaborides which differs from that for a semiconductor. This difference is reflected in the equilibrium lattice constant, which is given by

$$a = a_0 + \eta\Delta r, \quad \eta = (\xi - 1)/\alpha\xi = \alpha C_r/(C_a + \alpha^2 C_r) . \tag{20}$$

In agreement with experiment, a follows the ionic radius[16] with $\eta \approx \frac{1}{2}$ according to the variation in lattice constant in the rare-earth metals (i.e., the ionic radius) and in the rare-earth hexaborides.

Using (20), we may evaluate η for the metallic hexaborides. We use the lattice constants and rare-earth ionic radii for PrB_6, GdB_6, Pr, and Gd to find that

$$\Delta a/\Delta r = \eta \approx 0.6 . \tag{21}$$

We take $\alpha \approx \frac{1}{2}$ as a reasonable estimate[27] and find that

$$\kappa_{SmB_6}/\kappa = (a_{SmB_6}/a)\xi \approx 1.4\,a_{SmB_6}/a . \tag{22}$$

Thus for PrB_6 (whose lattice constant is the same as that of SmB_6) we find a compressibility 1.4 times smaller than for SmB_6. Because the lattice constant varies by only 4%, our theory implies that SmB_6 has higher compressibility than the other rare-earth hexaborides.

V. LOW-TEMPERATURE SPECIFIC HEAT

The band structure of Fig. 3 suggests that the excitation of electrons across the gap E_1 and the corresponding movement of the Fermi level up into the conduction band will result in an interband contribution to the specific heat reminiscent of a Schottky anomaly. Depending upon the size of the residual p-type conductivity, moreover, we expect an intraband specific heat in the narrow valence band which will be large because of the high density of states involved. The high Debye temperature of the hexaboride lattice, and consequent small lattice specific heat at low temperatures, implies that these electronic contributions will be particularly pronounced.

We have measured the heat capacities of two SmB_6 samples, whose resistivity ratios $\rho_{4.2\,K}/\rho_{300\,K}$ were 60 (sample No. 19) and 800 (sample No. 22). Both samples were prepared by sintering boron and samarium in sealed tantalum crucibles and subsequent arc melting. Sample No. 22 is the same bar cut from the bulk whose transport properties are shown in Fig. 2.

Sample No. 22 ($\approx$90 mg) was measured using a dynamical-temperature-relaxation method which we have described elsewhere.[28] Measurements on

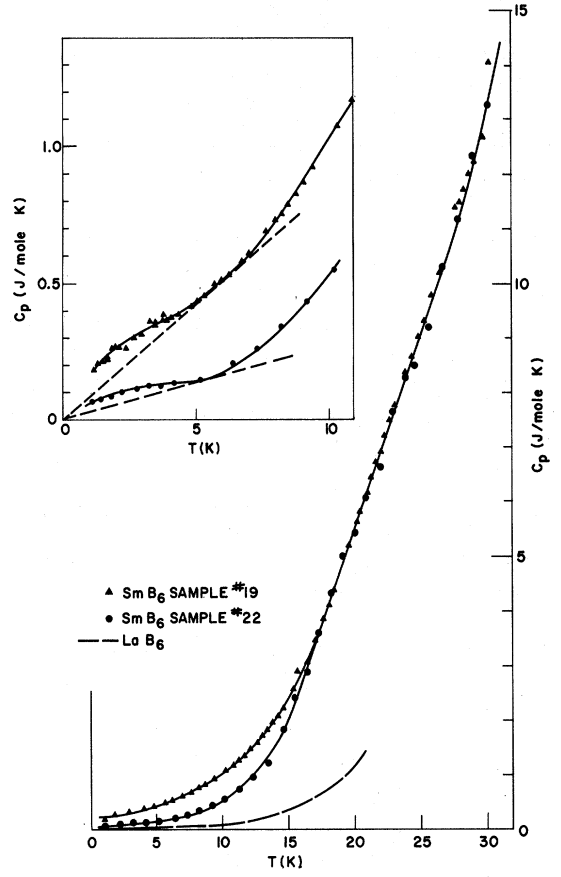

FIG. 6. Specific heat of SmB_6 in the range 1–30 K. Resistivity ratios: sample No. 19, 60; sample No. 22, 800. Insert: specific heat in the range 1–10 K.

sample No. 19 were made in two ways. The whole arc-melted button was used for a measurement by the pulse technique of Morin and Maita,[29] as part of an earlier investigation of the rare-earth hexaborides.[30] Later, we used a small chip (≈30 mg) of the button and extended the heat-capacity measurements down to 1 K. For the second measurement, we employed the temperature-relaxation technique. In the region of overlap the two sets of measurements agreed to better than their absolute accuracies of about 5%.

The data are presented in Fig. 6. Note that sample No. 19, which has higher residual conductivity, also has a larger low-temperature specific heat than sample No. 22. Note also that the specific heats of the two samples merge above 18 K. For comparison, we have included the specific heat of LaB_6,[30] an isostructural metal, to indicate the size of the lattice and conduction-electron specific heats in the metallic hexaborides. Below 10 K, it is negligible in comparison with the specific heat of SmB_6, and even at higher temperatures it does not rise as rapidly as our data do.

According to our interpretation of the transport data, the greater residual conductivity of sample No. 19 is due to a larger number of holes in the narrow valence band at $T=0$. We attribute the larger low-temperature specific heat of this sample to a larger intraband specific heat in the narrow valence band. As a rough approximation, we ignore the motion of the Fermi level and represent the electronic specific heat by a γT term, as shown in the insert of Fig. 6. This crude construction already allows us to correlate the specific heat and conductivity in interesting ways. Using the constant-mobility and effective-mass approximations for the narrow band, the values of γ may be related to the residual conductivities by

$$\gamma_{19}/\gamma_{22} = (\sigma_{19}/\sigma_{22})^{1/3} . \tag{23}$$

We find this relationship obeyed within 25%. Furthermore, an effective mass of 200 m_e is calculated, corresponding to a bandwidth of 100 K, consistent with the value we used to fit the transport data.

For both samples we find bumps peaked at roughly 3 K, reminiscent of Schottky anomalies. The fact that the peak occurs at such a small fraction of the energy gap $E_1(0)/k$ is surprising. The calculation of the theoretically predicted specific-heat anomaly is, however, complicated by the rapid low-temperature movement of the Fermi level. In fact, the motion of the Fermi level, which crosses into the conduction band at about 10 K, provides a reasonable explanation for the depression of the peak temperature to $\approx E_1/10k$. Preliminary calculations indicate that this effect may provide an explanation for our anomaly.

It should nevertheless be stressed that the bump may be due to other excitations in the SmB_6 system. The crystal field splitting of the bare $4f^5$ ground level, for example, is only about[18] 9 K; thermal excitation of these levels could contribute to our bump. Such an explanation has the added virtue that it explains in a natural way the scaling of the height of the bump with the residual conductivity (size of the $4f^5$ fraction at $T=0$) .

VI. CONCLUSION

The model of SmB_6 which we have discussed in Secs. I–V correlates all the experimental data known on this unusual material. The model is both complicated and apparently *ad hoc* in several ways, so that it seems desirable to summarize the range of correlations which we are able to achieve.

We have employed a model to describe SmB_6, including three basic concepts which are independent of, though consistent with, each other. Using an energy-band scheme with three bands, we have made a semiquantitative fit to the resistivity and Hall effect. This model also gives a qualitative

account of the thermopower measurements of Paderno *et al.*[8]

Quite apart from the transport behavior, we have explained the magnetic susceptibility[2] in quantitative detail by assuming the existence of the f^5s configuration. The remarkable feature of this configuration, that its ground state has no magnetic moment despite a nonzero total angular momentum, allows us to reconcile the magnetic properties with the x-ray absorption,[1] lattice constant,[3] and Mössbauer[4] data, which implied a temperature-independent mixture of $4f^6$ and $4f^5 f$ shells in the Sm ions in SmB_6.

This mixture of valences is the most strikingly anomalous feature of SmB_6. Our consideration of the competition between strain and ion configuration energies shows that the rigidity of the boron network may account for this behavior. On the basis of our simple lattice-energetics theory, we are able to account qualitatively for the temperature variation of the lattice constant.[3] Furthermore, we have found a relationship between the compressibilities of SmB_6 and the other rare-earth hexaborides.

In our view, then, the properties of SmB_6 arise as follows: The rigidity of the boron network, combined with the small energy difference between the $4f^6$ and $4f^5(5d\text{-}6s)$ configurations, leads to an equilibrium state containing a mixture of these ionic configurations. The fact that the ground state of the f^5s is nonmagnetic implies that the low-temperature susceptibility of SmB_6 is of the Van Vleck temperature-independent type, as observed.[2]

The transport properties of the ionic levels responsible for the magnetic behavior are describable in terms of a narrow band with temperature-dependent energy. Together with a valence band comprised of boron bonding states and a conduction band made up of Sm-related $5d$-$6s$ states, we have a three-band model which describes the transport properties.

The low-temperature specific heat is qualitatively related to the transport behavior, in that the large electronic contribution to the specific heat can be correlated with conduction in a narrow band.

Despite the complexity of such a model, we believe that the range of data described by it justify our belief that we have given a valid description of SmB_6.

ACKNOWLEDGMENTS

We are grateful to E. Buehler for his considerable contribution in helping us to improve the stoichiometry of the bulk samples, to A. Menth for many useful conversations, and to S. Curry for assistance in computer programming. The able technical assistance of H.-U. Thomas is gratefully acknowledged.

APPENDIX

In this Appendix, we describe the band properties of the localized $5de_g$-$6s$ electrons. The electron states which make up the ionic configuration are highly correlated because of the exchange and spin-orbit interactions which give rise to the level scheme. In such a case, the free-electron-like single-particle approximation which is normally used to describe electron bands fails. Nevertheless, one can describe the transport properties of such electrons within the framework of band theory. The necessary modification is that the energy band be dependent upon the relative populations of the ionic configurations; that is, the band gap is temperature dependent.

We write the grand canonical partition function for the system, explicitly including both ionic and conduction-band states. For this purpose we divide the ionic states into divalent ($4f^6$ and f^5s) and trivalent ($4f^5$) families, denoting the energies and degeneracies of the divalent states by (E_{2i}, g_{2i}), and those of the trivalent states (E_{3i}, g_{3i}). We may then write the total partion function as the product

$$Z = Z_{\text{cond}}\, Z_{\text{ion}}\,, \tag{A1}$$

where

$$Z_{\text{cond}} = \prod_{\vec{k}} \left[1 + e^{-[\epsilon(\vec{k})-\epsilon_F]/kT}\right] \tag{A2a}$$

and

$$Z_{\text{ion}} = \prod_{\text{all Sm sites}} \left(\sum_i g_{2i} e^{-(E_{2i}-n_2\epsilon_F)/kT} + \sum_j g_{3j} e^{-(E_{3j}-n_3\epsilon_F)/kT} \right). \tag{A2b}$$

n_2 (equal to 60) is the total number of electrons on a divalent Sm ion, and n_3 (equal to 59) is the number on a trivalent ion.

We also write the single-ion partition functions

$$Z_2 = \textstyle\sum_i g_{2i}\, e^{-E_{2i}/kT} \quad \text{and} \quad Z_3 = \sum_j g_{3j}\, e^{-E_{3j}/kT}\,, \tag{A3}$$

which would represent the ionic configuration completely if there were no possibility of divalent-to-trivalent transitions. Z_2, of course, is the sum of the partition functions of the $4f^6$ and f^5s configurations.

Putting (A3) into (A2b), we find that

$$Z_{\text{ion}} = \left[1 + (Z_2/Z_3)\, e^{\epsilon_F/kT}\right]^N (Z_3\, e^{n_3\epsilon_F/kT})^N\,, \tag{A4}$$

where N is the total number of Sm sites. By analogy with the usual partition function for a degenerate Fermi gas (A2a), we may identify the first factor in (A4) as the partition function of an N-fold-degenerate level with an energy given by

$$E(T) = -kT\ln(Z_2/Z_3) = -kT\ln\left(\frac{\sum_i g_{2i}\, e^{-E_{2i}/kT}}{\sum_j g_{3j}\, e^{-E_{3i}/kT}}\right), \tag{A5}$$

which is Eq. (7).

We thus have a total partition function (A1) which takes the form

$$Z = Z_{\text{level}}\, Z_{\text{trivalent ions}}\, Z_{\text{conduction band}}\,. \tag{A1'}$$

The narrow band, whose energy is temperature dependent, is the upper valence band of our transport model, and the conduction band contains the delocalized $5d$-$6s$ electrons which are ionized from divalent ions to form trivalent $4f^5$ ions. For computing the susceptibility, it is more convenient to consider the ion partition function in the form (A2b); the divalent ion states are thus implicity included in the Z_{level} factor in (A1').

---

†Research at Stanford was supported by the Advanced Research Projects Agency through the Center for Materials Research at Stanford University and by the U. S. Air Force Office of Scientific Research, Office of Aerospace Research, under Grant No. AFOSR 68-1510C.

*National Science Foundation Predoctoral Fellow.

‡Present address: Cavendish Laboratory, Cambridge University, Cambridge, U. K.

§Also at Joseph Henry Laboratory, Princeton University, Princeton, N. J. 08540. Kent Fellow of the Danforth Foundation.

‖Also at Department of Applied Physics, Stanford University, Stanford, Calif. 94305.

[1]E. E. Vainshtein, S. M. Blokhin, and Yu. B. Paderno, Fiz. Tverd. Tela 6, 2909 (1964) [Soviet Phys. Solid State 6, 2318 (1965)].

[2]A. Menth, E. Buehler, and T. H. Geballe, Phys. Rev. Letters 22, 295 (1969).

[3]A. Menth, E. Buehler, H. J. Levinstein, and T. H. Geballe, J. Appl. Phys. 40, 1006 (1969).

[4]R. L. Cohen, M. Eibschütz, and K. W. West, Phys. Rev. Letters 24, 383 (1970); J. Appl. Phys. 41, 898 (1970).

[5]L. M. Falicov and J. C. Kimball, Phys. Rev. Letters 22, 997 (1969).

[6]J. M. Lafferty, J. Appl. Phys. 22, 299 (1951).

[7]T. H. Geballe, A. Menth, E. Buehler, and G. W. Hull, J. Appl. Phys. 41, 904 (1970).

[8]Yu. B. Paderno, V. I. Novikov, and E. S. Garf, J. Powder Metallurgy (USSR) 83, 70 (1969).

[9]H. C. Longuet-Higgins and M. deV. Roberts, Proc. Roy. Soc. (London) A224, 336 (1954).

[10]EuB_6 has only been made as a degenerate semiconductor. R. Bachmann, K. N. Lee, T. H. Geballe, and A. Menth, J. Appl. Phys. 41, 1431 (1970).

[11]Such as those found in NiO, for example. See A. J. Bosman, H. J. van Daal, and G. F. Kuvers, Phys. Letters 19, 372 (1965).

[12]Hall measurements just above T_c in ferromagnetic EuB_6 (Ref. 10) and through the ordering in the antiferromagnetic metal PrB_6 (unpublished data) show that in the case of ordering the ordinary Hall coefficient in the rare-earth hexaborides varies by less than 10%, with no changes of sign. In the metal, the Hall coefficient is consistent with the expected value of 1 electron per Pr ion.

[13]The influence of the high-mobility valence band will be to increase the mobility and thereby decrease the number of carriers.

[14]J. C. Nickerson (unpublished).

[15]Yu. B. Paderno, S. Pokrzywnicki, and B. Stalinski, Phys. Status Solidi 24, K73 (1967).

[16]B. Post, in *Boron, Metallo-Boron Compounds, Boranes*, edited by R. M. Adams (Interscience, New York, 1964).

[17]We are indebted to A. M. Clogston for suggesting this possibility to us.

[18]J. C. Nickerson, Ph. D. thesis, Stanford University, 1970 (unpublished).

[19]J. H. Van Vleck, *The Theory of Electric and Magnetic Susceptibilities* (Oxford, New York, 1959), Chap. IX.

[20]Although the $J=2$ ground level of the $f^5s\,\|$ is split by the cubic field, the moment of the crystal field states is still zero so long as we may ignore mixing in of the higher J levels by the crystal field potential. The 80 K splitting shown in Fig. 4 is the splitting between the lowest-lying crystal field states of the $f^5s\,\|$ and $f^5s\,\#$.

[21]One should note that a fit can be made which does not invoke the $f^5s\,\#$ term at all by slightly altering the $4f^6$:$4f^5$ ratio. This fit is somewhat worse at high temperatures than the one presented in Fig. 5. Nonetheless, both are approximate on account of the way we have chosen to parametrize the $f^5\|$-to-$f^5s\,\#$ mixing. Proper diagonalization of the spin-orbit term would thus show whether the bump is real, or an artifact of our calculation.

[22]J. L. Hoard and R. E. Hughes, in *The Chemistry of Boron and Its Compounds*, edited by E. L. Muetterties (Wiley, New York, 1967).

[23]R. W. Johnson and A. H. Daane, J. Chem. Phys. 38, 425 (1963).

[24]Properly speaking, of course, there are three configurations, the $4f^6$, f^5s, and $4f^5$. For the present considerations, however, we shall neglect the difference between f^5s and $4f^5$, since in both of these configurations the $5s$ and $5p$ orbitals which give rise to the ionic size are less well shielded than in the $4f^6$.

[25]The physical assumption that E_h has a minimum at (a_0, r_0) is expressed by the well-known criterion $C_r > 0$, $C_a > 0$.

[26]The boron-boron bond lengths within a boron octahedron are very close in length to those of the interoctahedral bonds. Taking a mean value of 1.72—1.74 Å for a boron-boron bond length, we find a lattice constant of 4.15—4.20 Å for an "ideal" hexaboride, quite close to the 4.133 Å measured in SmB_6 (see Ref. 22).

[27]$\alpha = \frac{1}{2}$ corresponds to $2\alpha r$ equal to the ionic radius in the rare-earth metal, a relation which is satisfied to within about 10% for all the rare-earth hexaborides including SmB_6. This condition may be deduced from a detailed consideration of the spring model (see Ref. 18).

[28]K. N. Lee, R. Bachmann, T. H. Geballe, and J. P. Maita, Phys. Rev. B 2, 4580 (1970).

[29]F. J. Morin and J. P. Maita, Phys. Rev. 129, 1115 (1963).

[30]B. T. Matthias, T. H. Geballe, K. Andres, E. Corenzwit, G. W. Hull, and J. P. Maita, Science 159, 530 (1968); T. H. Geballe, B. T. Matthias, K. Andres, J. P. Maita, A. S. Cooper, and E. Corenzwit, *ibid.* 160, 1443 (1968).

PHYSICAL REVIEW B VOLUME 3, NUMBER 6 15 MARCH 1971

Localized Defects in PbTe†

Nelson J. Parada*
Materials Theory Group, Department of Electrical Engineering, Massachusetts Institute of Technology, Cambridge, Massachusetts 02139
(Received 20 April 1970)

The electronic energy levels associated with vacancies in PbTe are obtained through the Green's-function method of Koster and Slater, the unperturbed Bloch functions being obtained from a relativistic $\vec{K}\cdot\vec{\pi}$ augmented-plane-wave (APW) energy-band calculation. APW one-electron energies were obtained at Γ and the corresponding eigenfunctions were used to obtain matrix elements of the relativistic momentum operator $\vec{\pi}$ between states at Γ. These energies and matrix elements were used in a $\vec{K}\cdot\vec{\pi}$ secular equation to obtain energies and wave functions at approximately 4300 points in the Brillouin zone. With 11 relativistic bands at Γ, excellent results were obtained. Localized Wannier functions were constructed by taking suitable linear combinations of the unperturbed Bloch functions and these Wannier functions provided the basis in which the energy levels in the presence of the perturbing impurity potential were found. We have solved the vacancy problem using Wannier functions from nine bands (five valence and four conduction) and 13 lattice sites. The results obtained from this calculation showed that Pb vacancies produce p-type PbTe, whereas Te vacancies produce n-type PbTe, and in both cases, carriers are present at all temperatures.

I. INTRODUCTION

It is our intention here to present a detailed account of the previously published calculation of the energy levels associated with vacancies in PbTe.[1] Lead telluride is known to have a NaCl crystal structure with a lattice constant of 6.452 Å (12.193 a.u.)[2] and to be a semiconductor with a direct gap of about 0.3 eV at room temperature.[3] The gap is located at the L point in the Brillouin zone. The measured and calculated electronic properties of the lead salts have been recently reviewed by Prakash,[4] in his work on the measurements of the optical-absorption edge of these salts and its variation with temperature and pressure. A very interesting property of the lead chalcogenide group of semiconductors is that they have ranges of nonstoichiometry, the lattice incorporating either excess lead or chalcogen with the corresponding defects. While excess lead produces a n-type semiconductor, excess chalcogen gives rise to a p-type material. Both cases are characterized by high mobilities at liquid-helium temperatures and it is not possible to freeze out the carriers at low temperatures.[5] It has been found that for excess chalcogen the principal defect is a singly ionized lead vacancy while for excess lead, the situation is not yet clear: For PbSe it seems that the principal defect is a doubly ionized intersticial Pb,[6,7] while for PbS, a singly ionized sulfur vacancy appears to be the primary defect, although an appreciable concentration of doubly ionized intersticial Pb also exists.[8] On the other hand, a singly ionized tellurium vacancy is probably the most important defect in PbTe.[9] The theoretical study of vacancies in PbTe, therefore, presents the possibility of explaining the behavior described above.

The defect problem associated with a Pb and a Te vacancy is solved here in a manner similar to that used by Callaway and Hughes[10] for single and divacancies in silicon, that is, by applying the Green's-function method of Koster and Slater,[11] which has also been successfully used in the study of impurities in metals,[12] and in the problem connected with scattering of excitations in solids by localized imperfections.[13] The effect of the vacancy is treated as a time-independent localized potential and the perturbed wave functions are expanded in terms of Wannier functions of the unperturbed lattice. Because the latter functions are defined as linear combinations of Bloch functions, the knowledge of those wave functions, on a reasonable mesh of points in the Brillouin zone, is necessary.

The one-electron energy bands of PbTe were obtained by Conklin,[14] through a first-principles relativistic augmented-plane-wave (APW) calculation, and by Lin and Kleinman,[15] using a pseudopotential approach. Some experimental results can be very